Bulletin of the JSME Vol.10, No.5, 2023
Mechanical Engineering Journal

Substructure elimination method for vibration systems governed by a one-dimensional wave equation

Keisuke YAMADA* and Jinchen JI**
*Faculty of Engineering Science, Kansai University
3-3-35 Yamate-cho, Suita-shi, Osaka 564-8680, Japan
E-mail: yamadak@kansai-u.ac.jp
**School of Mechanical and Mechatronic Engineering, University of Technology Sydney
Ultimo, NSW 2007, Australia

Received: 6 June 2023; Revised: 20 July 2023; Accepted: 10 August 2023

Abstract
This paper presents a vibration analysis using the substructure elimination method for vibration systems governed by a one-dimensional wave equation. The utilization of a one-dimensional continuous body serves as a suitable approach for understanding the fundamental aspects of physical phenomena. Consequently, the significance of one-dimensional computer-aided engineering has witnessed a noticeable upsurge in recent years. The vibration analysis of continuous bodies through modal analysis is effective for reducing the degrees of freedom (DOFs). In addition, modal analysis of continuous bodies using the substructure elimination method can reduce the DOFs further, compared with modal analysis using the substructure synthesis method. However, the substructure elimination method was reported only briefly by the first author, and several problems remained. Focusing on continuous bodies governed by one-dimensional wave equations, this study aimed to address the aforementioned problems by devising solutions and establishing criteria for the effective utilization of the substructure elimination method. As a versatile method for setting arbitrary boundary conditions, a new formulation method based on constraint conditions was proposed. In addition, appropriate material properties of the elimination regions and highest order of the eigenmode were determined through a simulation-based investigation. The effectiveness of the substructure elimination method was verified by comparing the simulation results obtained using the substructure elimination method and exact solutions obtained using the boundary conditions. To investigate the advantage of low DOFs, the simulation results obtained using the substructure elimination method were also compared with those obtained using the substructure synthesis method. As an example, in a simulation of a 0.85 m one-dimensional acoustic field with a non-reflective boundary, highly precise results were obtained below 1200 Hz using 15 DOFs and the substructure elimination method.

Keywords : Acoustic field, Wave equation, Modal analysis, Coupled vibration, Continuum vibration, Simulation, Displacement excitation, Non-reflective boundary

1. Introduction

Vibration simulation technology has advanced significantly with the development of computer technology. Improving the accuracy of vibration simulations reduces the need for prototyping equipment. The development of numerical analysis methods, such as the finite element method, has enabled the analysis of the vibration of a continuous body with a multidimensional complex shape. Although improving the precision of these vibration analyses is an important research topic for vibration engineering, vibration analysis that uses a spring mass system with low degrees of freedom (DOFs) or a one-dimensional continuous body proves to be advantageous in understanding the fundamental nature of the physical phenomenon and is effective during the conceptual design stage. Therefore, one-dimensional computer-aided engineering (1D CAE) is important (Ohtomi, 2015). In this study, we focused on a vibration analysis method for a one-dimensional continuous body that can be used for 1D CAE. There are two types of one-dimensional continuous bodies that are particularly important in vibration engineering: one is those governed by one-dimensional

Paper No.23-00241
J-STAGE Advance Publication date : 23 August, 2023
[DOI: 10.1299/mej.23-00241]

wave equations, such as thin acoustic tubes and strings, and the other is those governed by fourth-order partial differential equations, such as the bending vibration of a beam. Because the governing equations of the two types differ significantly, only the first is described here. In this study, a one-dimensional acoustic field is used as the representative analysis object. This analysis method can be applied to any vibration system whose governing equation is a one-dimensional wave equation.

There are several methods for analytically deriving the sound pressure and particle displacement in a one-dimensional acoustic field. The most typical method is to determine the coefficients of the expression that satisfy the wave equation based on the boundary conditions (Bishop and Johnson, 1960; Tanaka et al., 2012). An extension of this method is the transfer matrix method (Uhrig, 1966; Jiménez et al., 2021). It can be used to analyze, for example, an acoustic tube with branches. Although these methods provide exact solutions, these are incapable of obtaining equations of motion with low DOFs. To address this problem, Yamada and Utsuno (2015, 2020) proposed a method for applying modal analysis to a one-dimensional acoustic field with vibrating boundaries. In this method, the displacement excitation at the boundary is replaced equivalently with a rigid wall and sound pressure source. Using this method, the substructure synthesis method can be applied (Hale and Meirovitch, 1980; Ookuma and Nagamatsu, 1985, 1986; Shabana, 1985). For example, the governing equations of an acoustic tube with a side-branch silencer or Helmholtz silencer can be expressed by 2-DOF equations of motion (Yamada et al., 2021a, 2021b). In these methods, the optimum tuning conditions for the silencers could be formulated because the DOFs were two. Moreover, this method is better than the transfer matrix method in that the effect of the width of the branched acoustic tube can be considered, and the equations of motion of vibration systems with feedback control can be formulated conveniently (Shigeno and Yamada, 2022). This method can also be used to analyze coupled vibrations between acoustic fields and structures (Yamada and Utsuno, 2015). In the vibration analysis of a continuous body by modal analysis (Benaroya and Nagurka, 2009; Meirovitch, 1967, 1990, 2001; Nagamatsu, 1985; Rao, 2007; Reismann, 1988; Shabana, 1991), exact solutions are obtained if all the infinite eigenmodes of the continuous body can be considered. In practice, higher-order eigenmodes are typically omitted because only a finite number of eigenmodes can be included. Consequently, the results obtained by modal analysis are approximate solutions. Even if the objective is not to obtain equations of motion with low DOFs as described above, it is better to obtain approximate solutions with sufficient precision and fewer DOFs. From this perspective, the analysis method of replacing the displacement excitation with a rigid wall and sound pressure source is not advantageous.

The first author proposed the substructure elimination method as a theoretical method for analyzing the vibration of a continuous body based on a concept different from that of the substructure synthesis method (Yamada, 2017, 2018). In the substructure synthesis method, the governing equations of the entire vibration system are obtained by adding substructures (Hale and Meirovitch, 1980; Ookuma and Nagamatsu, 1985, 1986; Shabana, 1985). In the substructure elimination method, the substructures are eliminated from a single overall structure. Modal analysis is also used in this method. The method requires fewer DOFs than the substructure synthesis method, particularly in multidimensional vibration systems. This is because only the superposition of the eigenmodes of the original overall structure is used to express the vibration of the entire vibration system. Conversely, the substructure synthesis method requires the superposition of the eigenmodes in each substructure. Although this advantage is less effective in one-dimensional vibration systems, another advantage is that it reduces the DOFs in one-dimensional vibration systems using the substructure elimination method. For example, when analyzing the coupled vibration of a one-dimensional acoustic field and 1-DOF vibration system comprising a mass point, spring, and dashpot, the method of replacing the displacement excitation with a rigid wall and sound pressure source installs a 1-DOF vibration system at the boundary of the acoustic field. In the substructure elimination method, a 1-DOF vibration system is installed inside the original acoustic field. This difference in the spatial coordinates is important. In the first method, the phases of the eigenfunctions determined by the spatial coordinate of the 1-DOF vibration system are in phase or antiphase for all the eigenmodes. In the second method, the phases have different values for each eigenmode. The vibration at the coordinate of the 1-DOF vibration system should be expressed by the superposition of the original eigenmodes. The second method can tune the amplitude and phase with fewer eigenmodes because of the phase variation.

Thus, the substructure elimination method is likely to be effective for analyzing one-dimensional vibration systems as well. However, this method is reported only briefly by the first author, and several problems remain. First, a versatile method for setting arbitrary boundary conditions on new boundaries is not provided. Second, the criteria for determining the density, bulk modulus, and length of the elimination region are not provided. Third, a criterion for determining the highest order of the eigenmode when the upper limit of the frequency range is given is not provided. Therefore, to solve

[DOI: 10.1299/mej.23-00241]

the first problem, this study proposes a new formulation method based on constraint conditions. Modal analysis is applied to the obtained wave equation, and equations of motion using modal displacements are derived. To solve the second and third problems, the appropriate material properties of the elimination region and the highest order of the eigenmode are determined through simulations. In particular, the appropriate length of the elimination region is investigated using the wavelength of the highest order eigenmode as the criterion because the phases of the eigenfunctions at the new boundary are important. In this study, the effectiveness of the substructure elimination method is verified by comparing the simulation results obtained using the substructure elimination method with the exact solutions obtained using boundary conditions. To investigate the advantages of low DOFs, the simulation results obtained using the substructure elimination method are also compared with the simulation results obtained using the substructure synthesis method.

2. Theoretical analysis

In this study, a one-dimensional acoustic field was used as a representative vibration system governed by a one-dimensional wave equation. We describe an analysis method for eliminating the regions at both ends of the original acoustic field and providing new boundaries to the new ends using constraint conditions. This elimination of the regions provides variation in the phase of each eigenmode at the new boundaries. Four types of boundaries are described: free end, closed end, displacement excitation, and arbitrary mechanical impedance using a 1-DOF vibration system. After deriving the wave equation under each boundary condition, modal analysis is conducted to derive the equations of motion using modal displacements. The vibration in the acoustic field is expressed by the superposition of the eigenmodes of the original acoustic field in modal analysis before the regions at both the ends are eliminated.

Equations of motion with low DOFs can be obtained using modal analysis. If branched acoustic tubes are installed on a host acoustic tube, the effect of the widths of the branched acoustic tubes can be considered, and equations of motion of the vibration systems with feedback control can be derived conveniently using modal analysis. These cannot be implemented by the method described in Section 3.4.2, which uses boundary conditions to derive exact solutions. However, modal analysis without substructure elimination method requires more DOFs to maintain accuracy. The phase variation in the substructure elimination method reduces the required DOFs.

2.1 Analytical model

The analytical model of a one-dimensional acoustic field is shown in Fig. 1(a). Here, the cross-sectional area of the acoustic field is uniform and is S; the lengths of the center region and left and right elimination regions are l_{A}, l_{B}, and l_{C}, respectively; their air densities are ρ_{A}, ρ_{B}, and ρ_{C}, respectively; their bulk moduli are κ_{A}, κ_{B}, and κ_{C}, respectively; the left end of the acoustic field is set to the origin of the x-coordinate; and the right-hand direction is the positive direction of the x-coordinate. The x-coordinates of the new left and right boundaries are $x_{\mathrm{B}}\left(=l_{\mathrm{B}}\right)$ and $x_{\mathrm{C}}\left(=l_{\mathrm{A}}+l_{\mathrm{B}}\right)$, respectively, and the overall length of the acoustic field is $l_{\mathrm{ABC}}\left(=l_{\mathrm{A}}+l_{\mathrm{B}}+l_{\mathrm{C}}\right)$. The center region and left and right elimination regions are referred to as regions A, B, and C, respectively. In this study, only the cases with $\rho_{\mathrm{B}}=\rho_{\mathrm{C}}$ and $\kappa_{\mathrm{B}}=\kappa_{\mathrm{C}}$ were considered because regions B and C were eliminated in a similar manner. However, in the formulation, the symbols for air densities and bulk moduli were separated to clearly distinguish between regions B and C. As shown in Fig. 1(a), the external forces f_{B} and f_{C} are applied to the new left and right boundaries in the right-hand direction. These are determined by the constraint conditions. In this study, eliminating a region implies that the air density and bulk modulus of the region are set to zero or sufficiently small values such that the sound pressure is zero or

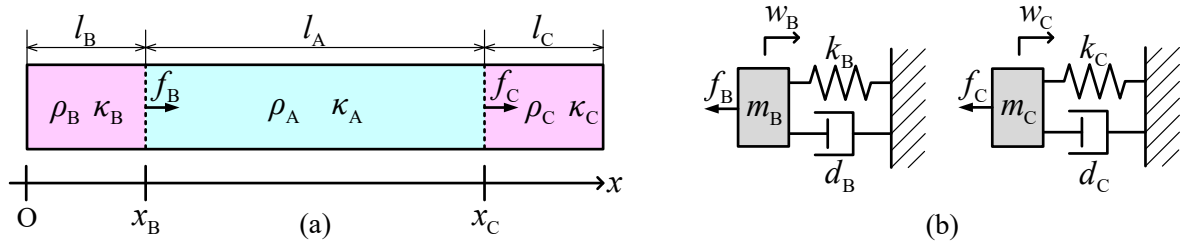

Fig. 1 Analytical models of a one-dimensional acoustic field and 1-DOF vibration systems used in the substructure elimination method: (a) analytical model of a one-dimensional acoustic field and (b) analytical models of 1-DOF vibration systems installed at $x=x_{\mathrm{B}}$ and x_{C}.

[DOI: 10.1299/mej.23-00241]

almost zero in that region. Although the sound pressure is zero in the elimination region, the particle displacement is not so. When the air density and bulk modulus in the elimination region are zero or sufficiently small, the sound pressure is zero or almost zero for all values of particle displacement. Therefore, the particle displacement can adopt any value in the elimination region. This is a convenient condition for expressing the vibration of the acoustic field by the superposition of the eigenmodes. The analytical models of the two 1-DOF vibration systems are shown in Fig. 1(b). These 1-DOF vibration systems provide an arbitrary mechanical impedance at new boundaries. The mass, spring constant, viscous damping coefficient, and displacement of the 1-DOF vibration system installed at $x = x_{\mathrm{B}}$ are m_{B}, k_{B}, d_{B}, and w_{B}, respectively, and those at $x = x_{\mathrm{C}}$ are m_{C}, k_{C}, d_{C}, and w_{C}, respectively. The positive direction of the displacements w_{B} and w_{C} is the right-hand direction. Because of the action and reaction relationship, f_{B} and f_{C} are applied to these mass points in the left-hand direction.

2.2 Wave equation and equations derived by constraint conditions

In general, the new left and right boundaries would have different constraints. However, in this section, the case in which the left and right boundaries have identical constraints is described to indicate the formulation of each constraint at the new left and right boundaries. Each formulation is combined when the left and right boundaries have different constraints.

2.2.1 Case where new boundary is set to free end

When the new boundaries are set to the free ends, $f_{\mathrm{B}} = 0$ and $f_{\mathrm{C}} = 0$ are given by the constraint conditions because the sound pressure should be zero at the free ends. The equation of motion of the minute fraction is expressed as

$$\rho(x)\frac{\partial^2 w}{\partial t^2} = -\frac{\partial p}{\partial x}, \tag{1}$$

$$\rho(x) = \rho_{\mathrm{A}} + \rho_{\mathrm{B\text{-}A}} H(x_{\mathrm{B}} - x) + \rho_{\mathrm{C\text{-}A}} H(x - x_{\mathrm{C}}), \quad \rho_{\mathrm{B\text{-}A}} = \rho_{\mathrm{B}} - \rho_{\mathrm{A}}, \quad \rho_{\mathrm{C\text{-}A}} = \rho_{\mathrm{C}} - \rho_{\mathrm{A}}, \tag{2}$$

where $\rho(x)$ is the density at the coordinate x, w is the particle displacement, t is time, p is the sound pressure, and H is the Heaviside step function. Multiplying both sides of Eq. (1) by the cross-sectional area of the acoustic field and the length of the minute fraction, dx, the term of the left-hand side is the inertial force of the minute fraction, and the term on the right-hand side is the force due to the differential pressure on both surfaces of the minute fraction. Because the sound pressure is proportional to the bulk strain, it is expressed as

$$p(x, t) = -\kappa(x)\frac{\partial w}{\partial x}, \tag{3}$$

$$\kappa(x) = \kappa_{\mathrm{A}} + \kappa_{\mathrm{B\text{-}A}} H(x_{\mathrm{B}} - x) + \kappa_{\mathrm{C\text{-}A}} H(x - x_{\mathrm{C}}), \quad \kappa_{\mathrm{B\text{-}A}} = \kappa_{\mathrm{B}} - \kappa_{\mathrm{A}}, \quad \kappa_{\mathrm{C\text{-}A}} = \kappa_{\mathrm{C}} - \kappa_{\mathrm{A}}, \tag{4}$$

where $\kappa(x)$ is the bulk modulus at the coordinate x. Equations (2) and (4) involve the Heaviside step functions. For example, the value of $H(x_{\mathrm{B}} - x)$ at $x = x_{\mathrm{B}}$ should be determined as follows. When considering regions A and B, $x = x_{\mathrm{B}} + 0$ and $x = x_{\mathrm{B}} - 0$ should be used, respectively. The values of $H(x_{\mathrm{B}} - x)$ in regions A and B are 0 and 1, respectively. Introducing the displacement potential ψ, the particle displacement w can be expressed as

$$w(x, t) = -\frac{\partial \psi}{\partial x}. \tag{5}$$

Substituting Eqs. (3) and (5) into Eq. (1) and integrating both the sides with respect to x, the following wave equation is obtained:

$$\rho(x)\frac{\partial^2 \psi}{\partial t^2} - \rho_{\mathrm{B\text{-}A}} H(x_{\mathrm{B}} - x)\frac{\partial^2 \psi}{\partial t^2}\bigg|_{x=x_{\mathrm{B}}} - \rho_{\mathrm{C\text{-}A}} H(x - x_{\mathrm{C}})\frac{\partial^2 \psi}{\partial t^2}\bigg|_{x=x_{\mathrm{C}}} = \kappa(x)\frac{\partial^2 \psi}{\partial x^2}. \tag{6}$$

The velocity potential is generally used in the wave equation of an acoustic field. The velocity potential is derived using

[DOI: 10.1299/mej.23-00241]

$\partial\psi/\partial t$. Although the displacement potential ψ is used, the particle velocity can be obtained conveniently. Moreover, the formulation using ψ is more straightforward than that using the velocity potential. This is particularly the case when a 1-DOF vibration system is installed on the new boundary.

When the longitudinal vibration of a thin rod is analyzed, Young's modulus should be used rather than bulk modulus in Eq. (6). When the vibration of a string is analyzed, linear density and tension should be used rather than density and bulk modulus, respectively. The displacement potential can be used in both cases if the boundary conditions of the original rod and string are assumed to be rigid walls. Equation (5) can be used to derive the displacement of the rod and deflection of the string in each case.

2.2.2 Case where new boundary is set to closed end or displacement excitation

When the new boundaries are set to closed ends, the particle displacement at the new boundaries should be zero. When the new boundaries are set for displacement excitation, the particle displacements at the new boundaries should be equal to the displacement. The first of these can be considered a special case in which the displacement is zero. To satisfy the constraint conditions, f_B and f_C are applied to the acoustic field at $x=x_\mathrm{B}$ and x_C, respectively. Therefore, in these cases, the external force terms are added to the wave equation (6) as follows:

$$\rho(x)\frac{\partial^2\psi}{\partial t^2}-\rho_{\mathrm{B\text{-}A}}H(x_\mathrm{B}-x)\frac{\partial^2\psi}{\partial t^2}\bigg|_{x=x_\mathrm{B}}-\rho_{\mathrm{C\text{-}A}}H(x-x_\mathrm{C})\frac{\partial^2\psi}{\partial t^2}\bigg|_{x=x_\mathrm{C}}=\kappa(x)\frac{\partial^2\psi}{\partial x^2}+\frac{f_\mathrm{B}}{S}H(x_\mathrm{B}-x)-\frac{f_\mathrm{C}}{S}H(x-x_\mathrm{C}). \tag{7}$$

The second and third terms on the right-hand side of Eq. (7) are for the external forces f_B and f_C, respectively. These can be replaced by $-f_\mathrm{B}H(x-x_\mathrm{B})/S$ and $f_\mathrm{C}H(x_\mathrm{C}-x)/S$, respectively. Partial differentiation of both sides of the wave equation (7) with respect to x yields the dimensions of the equation of motion given by Eq. (1). For example, $f_\mathrm{B}H(x_\mathrm{B}-x)/S$ and $-f_\mathrm{B}H(x-x_\mathrm{B})/S$ provide an identical expression when these are partially differentiated with respect to x. Any terms could be used in Eq. (7) if these are equal in the dimensions of Eq. (1). This is because, to obtain the sound pressure, only the pressure variation is required, and a constant pressure corresponding to the integration constant is not required. It is advantageous to provide the external force terms using the two terms in Eq. (7) in that the external force terms are not included when deriving the sound pressure in region A.

Equation (7) contains two unknown variables, f_B and f_C, and two equations are required to determine these. Therefore, these are given by the constraint conditions at the new left and right boundaries as follows:

$$w(x_\mathrm{B},t)=-\frac{\partial\psi}{\partial x}\bigg|_{x=x_\mathrm{B}}=w_\mathrm{L}(t), \tag{8}$$

$$w(x_\mathrm{C},t)=-\frac{\partial\psi}{\partial x}\bigg|_{x=x_\mathrm{C}}=w_\mathrm{R}(t), \tag{9}$$

where w_L and w_R are the displacements imposed by the pistons at the new left and right boundaries, respectively. When closed ends are installed rather than displacement excitation, $w_\mathrm{L}=0$ and $w_\mathrm{R}=0$ should be used in Eqs. (8) and (9), respectively.

2.2.3 Case where arbitrary mechanical impedance is installed at new boundary

When the 1-DOF vibration systems shown in Fig. 1(b) are installed at the new left and right boundaries, the wave equation is given by Eq. (7). The two equations for determining the unknown variables f_B and f_C are given by the equations of motion for the two 1-DOF vibration systems as follows:

$$m_\mathrm{B}\ddot{w}_\mathrm{B}+d_\mathrm{B}\dot{w}_\mathrm{B}+k_\mathrm{B}w_\mathrm{B}=-f_\mathrm{B},\quad m_\mathrm{C}\ddot{w}_\mathrm{C}+d_\mathrm{C}\dot{w}_\mathrm{C}+k_\mathrm{C}w_\mathrm{C}=-f_\mathrm{C}. \tag{10}$$

Because displacements w_B and w_C are unknown variables, these need to be determined by the constraint conditions. In this case, w_B and w_C should be equal to the particle displacements at $x=x_\mathrm{B}$ and x_C. Therefore, the following equations are derived:

[DOI: 10.1299/mej.23-00241]

$$w_{\mathrm{B}}=-\left.\frac{\partial\psi}{\partial x}\right|_{x=x_{\mathrm{B}}},\quad w_{\mathrm{C}}=-\left.\frac{\partial\psi}{\partial x}\right|_{x=x_{\mathrm{C}}}. \tag{11}$$

2.3 Modal analysis

As described in Section 2.2, the wave equation is identical in all the cases, and the external forces f_{B} and f_{C} differ for each new boundary condition. In this section, modal analysis is first applied to wave equation (7). Then, the external forces f_{B} and f_{C} are expressed as a superposition of the eigenmodes.

In the substructure elimination method, ψ is obtained by the superposition of the eigenmodes before eliminating regions B and C. That is, using the eigenmodes when the densities and bulk moduli of regions B and C are ρ_{A} and κ_{A}, respectively, ψ can be expressed as

$$\psi(x,t)=\sum_{h=0}^{n}\Psi_h(x)\xi_h(t),\quad \Psi_h(x)=A_h\cos k_h x,\quad k_h=\frac{h\pi}{l_{\mathrm{ABC}}}, \tag{12}$$

where Ψ_h is the eigenfunction of the displacement potential, ξ_h is the modal displacement, the subscript h denotes the hth-order eigenmode, n is the highest order of the eigenmode, A_h is the arbitrary constant, and k_h is the wave number. Eigenmodes are also referred to as acoustic or vibration modes in the literature. Equation (12) is a Fourier cosine series. Substituting Eq. (12) into the wave equation (7), multiplying both the sides by Ψ_i/ρ_{A}, and integrating over the entire range of the acoustic field, we obtain the following equations of motion using modal displacements:

$$\begin{aligned}&M_i\ddot{\xi}_i+\frac{\rho_{\text{B-A}}}{\rho_{\mathrm{A}}}\sum_{h=0}^{n}\left(\int_0^{x_{\mathrm{B}}}\Psi_h\Psi_i\mathrm{d}x-\Psi_h(x_{\mathrm{B}})\int_0^{x_{\mathrm{B}}}\Psi_i\mathrm{d}x\right)\ddot{\xi}_h+\frac{\rho_{\text{C-A}}}{\rho_{\mathrm{A}}}\sum_{h=0}^{n}\left(\int_{x_{\mathrm{C}}}^{l_{\mathrm{ABC}}}\Psi_h\Psi_i\mathrm{d}x-\Psi_h(x_{\mathrm{C}})\int_{x_{\mathrm{C}}}^{l_{\mathrm{ABC}}}\Psi_i\mathrm{d}x\right)\ddot{\xi}_h\\&+K_i\xi_i+\frac{\kappa_{\text{B-A}}}{\rho_{\mathrm{A}}}\sum_{h=1}^{n}k_h^2\int_0^{x_{\mathrm{B}}}\Psi_h\Psi_i\mathrm{d}x\xi_h+\frac{\kappa_{\text{C-A}}}{\rho_{\mathrm{A}}}\sum_{h=1}^{n}k_h^2\int_{x_{\mathrm{C}}}^{l_{\mathrm{ABC}}}\Psi_h\Psi_i\mathrm{d}x\xi_h-\frac{f_{\mathrm{B}}}{\rho_{\mathrm{A}}S}\int_0^{x_{\mathrm{B}}}\Psi_i\mathrm{d}x+\frac{f_{\mathrm{C}}}{\rho_{\mathrm{A}}S}\int_{x_{\mathrm{C}}}^{l_{\mathrm{ABC}}}\Psi_i\mathrm{d}x=0\end{aligned}, \tag{13}$$

$$M_i=\int_0^{l_{\mathrm{ABC}}}\Psi_i^2\mathrm{d}x=1,\quad K_i=-c_{\mathrm{A}}^2\int_0^{l_{\mathrm{ABC}}}\Psi_i\frac{\mathrm{d}^2\Psi_i}{\mathrm{d}x^2}\mathrm{d}x=\omega_i^2,\quad c_{\mathrm{A}}=\sqrt{\frac{\kappa_{\mathrm{A}}}{\rho_{\mathrm{A}}}},\quad \omega_i=\frac{i\pi c_{\mathrm{A}}}{l_{\mathrm{ABC}}},\quad A_i=\begin{cases}\sqrt{\dfrac{1}{l_{\mathrm{ABC}}}} & (i=0)\\ \sqrt{\dfrac{2}{l_{\mathrm{ABC}}}} & (i=1,2,\cdots)\end{cases}, \tag{14}$$

where M_i and K_i are the modal mass and modal stiffness, respectively, of the original acoustic field without elimination; c_{A} is the sound speed in region A; and ω_i is the natural angular frequency of the ith-order eigenmode of the original acoustic field. The wavenumber k_i and natural angular frequency ω_i have the relationship $k_i=\omega_i/c_{\mathrm{A}}$. The arbitrary constant A_i of the eigenfunction was normalized so that $M_i=1$ in this study. The second and fifth terms of the left-hand side of Eq. (13) are the results of the elimination of region B. The third and sixth terms are the results of the elimination of region C. The seventh and eighth terms on the left-hand side of Eq. (13) are terms of the external forces applied by the constraints at the new left and right boundaries, respectively. The equation of motion using matrices is expressed as

$$[M]\{\ddot{\xi}\}+[K]\{\xi\}+[Q]\{f\}=\{0\},\quad \{\xi\}=\{\xi_0\quad \xi_1\quad \cdots\quad \xi_n\}^{\mathrm{T}},\quad \{f\}=\{f_{\mathrm{B}}\quad f_{\mathrm{C}}\}^{\mathrm{T}}, \tag{15}$$

where $[M]$ is the mass matrix, which is a square matrix of size $n+1$; $[K]$ is the stiffness matrix, which is a square matrix of size $n+1$; $[Q]$ is the external force influence matrix, which is an $(n+1)$-by-2 matrix; $\{\xi\}$ is the modal displacement vector; $\{f\}$ is the external force vector; and the superscript T denotes the transpose of the matrix. Each element of matrices $[M]$, $[K]$, and $[Q]$ can be obtained using Eq. (13).

When both the new boundaries are set at the free ends, $\{f\}=\{0\quad 0\}^{\mathrm{T}}$. Therefore, the following equation is obtained:

$$[M]\{\ddot{\xi}\}+[K]\{\xi\}=\{0\}. \tag{16}$$

[DOI: 10.1299/mej.23-00241]

When both the new boundaries are set to the displacement excitation, from Eqs. (8), (9), and (12), the equations given by the constraint conditions are expressed as

$$-\sum_{h=1}^{n}\left.\frac{\mathrm{d}\Psi_h}{\mathrm{d}x}\right|_{x=x_\mathrm{B}}\xi_h = w_\mathrm{L}(t),\quad -\sum_{h=1}^{n}\left.\frac{\mathrm{d}\Psi_h}{\mathrm{d}x}\right|_{x=x_\mathrm{C}}\xi_h = w_\mathrm{R}(t). \tag{17}$$

Equations (15) and (17) can be used to numerically derive the modal displacements. However, the eigenvalue analysis cannot be performed using Eq. (17). If terms $\ddot{f}_\mathrm{B}$ and $\ddot{f}_\mathrm{C}$ are added to Eq. (17) such that the coefficients are sufficiently small to be omitted, an eigenvalue analysis can be performed. However, the problem remains that these coefficients should be selected appropriately. To solve this problem, the particle displacement $w(x,t)$ should be expressed using f_B or f_C. Integrating both sides of wave equation (7) from $x=0$ to x, where $x_\mathrm{B}\le x\le x_\mathrm{C}$, we obtain the following equation for particle displacement:

$$w(x,t) = -\frac{\partial\psi}{\partial x} = -\frac{\rho_\mathrm{A}}{\kappa_\mathrm{A}}\int_0^x\frac{\partial^2\psi}{\partial t^2}\mathrm{d}x - \frac{\rho_\mathrm{B\text{-}A}}{\kappa_\mathrm{A}}\int_0^{x_\mathrm{B}}\frac{\partial^2\psi}{\partial t^2}\mathrm{d}x + \frac{\rho_\mathrm{B\text{-}A}}{\kappa_\mathrm{A}}l_\mathrm{B}\left.\frac{\partial^2\psi}{\partial t^2}\right|_{x=x_\mathrm{B}} + \frac{\kappa_\mathrm{B\text{-}A}}{\kappa_\mathrm{A}}\left.\frac{\partial\psi}{\partial x}\right|_{x=x_\mathrm{B}} + \frac{l_\mathrm{B}}{\kappa_\mathrm{A}S}f_\mathrm{B}. \tag{18}$$

Integrating both sides of wave equation (7) from $x=x$ to l_ABC, where $x_\mathrm{B}\le x\le x_\mathrm{C}$, we obtain the following equation:

$$w(x,t) = -\frac{\partial\psi}{\partial x} = \frac{\rho_\mathrm{A}}{\kappa_\mathrm{A}}\int_x^{l_\mathrm{ABC}}\frac{\partial^2\psi}{\partial t^2}\mathrm{d}x + \frac{\rho_\mathrm{C\text{-}A}}{\kappa_\mathrm{A}}\int_{x_\mathrm{C}}^{l_\mathrm{ABC}}\frac{\partial^2\psi}{\partial t^2}\mathrm{d}x - \frac{\rho_\mathrm{C\text{-}A}}{\kappa_\mathrm{A}}l_\mathrm{C}\left.\frac{\partial^2\psi}{\partial t^2}\right|_{x=x_\mathrm{C}} + \frac{\kappa_\mathrm{C\text{-}A}}{\kappa_\mathrm{A}}\left.\frac{\partial\psi}{\partial x}\right|_{x=x_\mathrm{C}} + \frac{l_\mathrm{C}}{\kappa_\mathrm{A}S}f_\mathrm{C}. \tag{19}$$

From Eqs. (8) and (18), the equation given by the constraint condition at $x=x_\mathrm{B}$ is expressed as

$$-\frac{\rho_\mathrm{B}}{\kappa_\mathrm{A}}\int_0^{x_\mathrm{B}}\frac{\partial^2\psi}{\partial t^2}\mathrm{d}x + \frac{\rho_\mathrm{B\text{-}A}}{\kappa_\mathrm{A}}l_\mathrm{B}\left.\frac{\partial^2\psi}{\partial t^2}\right|_{x=x_\mathrm{B}} + \frac{\kappa_\mathrm{B\text{-}A}}{\kappa_\mathrm{A}}\left.\frac{\partial\psi}{\partial x}\right|_{x=x_\mathrm{B}} + \frac{l_\mathrm{B}}{\kappa_\mathrm{A}S}f_\mathrm{B} = w_\mathrm{L}(t). \tag{20}$$

Similarly, from Eqs. (9) and (19), the equation given by the constraint condition at $x=x_\mathrm{C}$ is derived as

$$\frac{\rho_\mathrm{C}}{\kappa_\mathrm{A}}\int_{x_\mathrm{C}}^{l_\mathrm{ABC}}\frac{\partial^2\psi}{\partial t^2}\mathrm{d}x - \frac{\rho_\mathrm{C\text{-}A}}{\kappa_\mathrm{A}}l_\mathrm{C}\left.\frac{\partial^2\psi}{\partial t^2}\right|_{x=x_\mathrm{C}} + \frac{\kappa_\mathrm{C\text{-}A}}{\kappa_\mathrm{A}}\left.\frac{\partial\psi}{\partial x}\right|_{x=x_\mathrm{C}} + \frac{l_\mathrm{C}}{\kappa_\mathrm{A}S}f_\mathrm{C} = w_\mathrm{R}(t). \tag{21}$$

From Eqs. (20) and (21), the equation using matrices is expressed as follows:

$$\left[M_f\right]\left\{\ddot{\xi}\right\} + \left[K_f\right]\left\{\xi\right\} + \left[Q_f\right]\left\{f\right\} = \left\{w\right\},\quad \left\{w\right\} = \left\{w_\mathrm{L}\quad w_\mathrm{R}\right\}^\mathrm{T}, \tag{22}$$

where each element of matrices $\left[M_f\right]$, $\left[K_f\right]$, and $\left[Q_f\right]$ can be determined using Eqs. (20) and (21). Eliminating the external force vector $\left\{f\right\}$ using Eqs. (15) and (22), the equations of motion using the matrices are expressed as

$$\left(\left[M\right]-\left[Q\right]\left[Q_f\right]^{-1}\left[M_f\right]\right)\left\{\ddot{\xi}\right\} + \left(\left[K\right]-\left[Q\right]\left[Q_f\right]^{-1}\left[K_f\right]\right)\left\{\xi\right\} = -\left[Q\right]\left[Q_f\right]^{-1}\left\{w\right\}. \tag{23}$$

When the new left and right boundaries are closed ends rather than displacement excitations, the term on the right-hand side of Eq. (23) is a zero vector. Using Eq. (23), eigenvalue analysis can be performed. Applying modal analysis to Eq. (23), we can obtain the uncoupled equations of motion.

Similarly, when 1-DOF vibration systems are installed at the new left and right boundaries, the external force vector $\left\{f\right\}$ should be expressed using modal displacements. From Eqs. (10) and (11), the following equations are derived:

[DOI: 10.1299/mej.23-00241]

$$m_{\mathrm{B}}\left.\frac{\partial^3\psi}{\partial t^2\partial x}\right|_{x=x_{\mathrm{B}}}+d_{\mathrm{B}}\left.\frac{\partial^2\psi}{\partial t\partial x}\right|_{x=x_{\mathrm{B}}}+k_{\mathrm{B}}\left.\frac{\partial\psi}{\partial x}\right|_{x=x_{\mathrm{B}}}=f_{\mathrm{B}},\quad m_{\mathrm{C}}\left.\frac{\partial^3\psi}{\partial t^2\partial x}\right|_{x=x_{\mathrm{C}}}+d_{\mathrm{C}}\left.\frac{\partial^2\psi}{\partial t\partial x}\right|_{x=x_{\mathrm{C}}}+k_{\mathrm{C}}\left.\frac{\partial\psi}{\partial x}\right|_{x=x_{\mathrm{C}}}=f_{\mathrm{C}}. \tag{24}$$

The particle displacements derived using Eqs. (5) and (12) should be used in Eq. (24). The particle displacements expressed by Eqs. (18) and (19) are unavailable here because the terms of the third- and fourth-order time derivatives appear. From Eq. (24), an equation using the matrices is derived as follows:

$$[M_m]\{\ddot{\xi}\}+[D_d]\{\dot{\xi}\}+[K_k]\{\xi\}=\{f\}, \tag{25}$$

where each element of the matrices $[M_m]$, $[D_d]$, and $[K_k]$ can be determined using Eq. (24). Substituting Eq. (25) into Eq. (15) yields the following equation:

$$\left([M]+[Q][M_m]\right)\{\ddot{\xi}\}+[Q][D_d]\{\dot{\xi}\}+\left([K]+[Q][K_k]\right)\{\xi\}=\{0\}. \tag{26}$$

When $[Q][D_d]$ is expressed as a linear sum of $[M]+[Q][M_m]$ and $[K]+[Q][K_k]$, i.e., when $[Q][D_d]$ is a Rayleigh damping, an eigenvalue analysis can be performed using Eq. (26). When $[Q][D_d]$ does not involve Rayleigh damping, eigenvalue analysis should be performed after deriving the equation of state from Eq. (26) for state-space representation. The uncoupled equations can be derived using eigenvectors.

The sound pressure and particle displacement in region A are important. From Eqs. (3), (5), and (7), the sound pressure in region A can be derived as

$$p(x,t)=\kappa_{\mathrm{A}}\frac{\partial^2\psi}{\partial x^2}=\rho_{\mathrm{A}}\frac{\partial^2\psi}{\partial t^2}, \tag{27}$$

The right-hand side of Eq. (27) has a zeroth-order eigenmode term. Consequently, it is marginally better than the middle portions of the equation, particularly in the low-frequency region. The particle displacement in region A is obtained as

$$w(x,t)=-\frac{\partial\psi}{\partial x}=-\sum_{h=1}^{n}\frac{\mathrm{d}\Psi_h}{\mathrm{d}x}\xi_h(t). \tag{28}$$

This equation is a Fourier sine series. The particle displacement can also be determined using Eq. (18) or (19). However, Eq. (28) becomes simpler. In the conventional method described in Section 3.4.3, the Gibbs phenomenon occurs when the particle displacement is derived using Eq. (28). However, the substructure elimination method does not address this issue. In the conventional method, the Gibbs phenomenon occurs because the eigenmodes do not exhibit particle displacement at either end. In contrast, the eigenmodes exhibit particle displacements at $x=x_{\mathrm{B}}$ and x_{C} when the substructure elimination method is used.

3. Verifications through simulation

In this section, the criteria for determining the density, bulk modulus, and length of the elimination region are established through simulations. Preferably, the density and bulk modulus in the elimination region are zero because the mechanical impedance of the elimination region is zero. Therefore, the case where the density and bulk modulus were zero and only the length of the elimination region was varied was first considered. Subsequently, the cases in which the density and bulk modulus had small values were considered. Furthermore, to obtain the criterion for determining the highest order n of the eigenmode of the original acoustic field, the precision of the natural frequencies obtained by eigenvalue analysis was investigated. In these simulations, the new boundary was either free or closed. To verify that the substructure elimination method requires fewer DOFs, the simulation results obtained when modal analysis was applied without using the substructure elimination method are also presented in this section. To verify whether the new boundary was a displacement excitation or 1-DOF vibration system, an acoustic tube with a displacement excitation at the left end

[DOI: 10.1299/mej.23-00241]

and 1-DOF vibration system at the right end was used in these simulations. Because these simulation results were compared with the exact solution derived using the boundary conditions, the derivation of the exact solution and the method of applying modal analysis without using the substructure elimination method are also described briefly.

3.1 Verification on the length of the elimination region

Two types of boundary conditions were used in the simulations to verify the lengths of the elimination regions. In one simulation, two new boundaries were set at the free ends. In the other simulation, these were set at the closed ends. The material properties used in the simulations are listed in Table 1. In these simulations, the relationship between the lengths of the elimination regions and the precision of the natural frequencies was evaluated. Lengths l_{B} and l_{C} of regions B and C were maintained equal in these simulations. Simulations were performed for three cases, namely, $n = 20$, 30, and 50 . The natural frequency of the highest order eigenmode of the original acoustic field varied with *n* and l_{ABC}. Regardless of whether the new boundaries were free or closed ends, the exact natural frequencies were integer multiples of 200 Hz. In these simulations, the root mean square (RMS) of the error rates of the natural frequencies obtained using the substructure elimination method was evaluated as the precision of the natural frequencies. The 1st–8th-order eigenmodes for $n = 20$, 1st–16th-order eigenmodes for $n = 30$, and 1st–32nd-order eigenmodes for $n = 50$ were used to calculate the RMS of the error rates of the natural frequencies. The simulation results for the two boundary conditions are shown in Figs. 2(a) and (b), respectively. The simulation results for the error rate of the first-order natural frequency are shown in Figs. 2(c) and (d), respectively. The error rate in Figs. 2(c) and (d) is the magnitude of the error rate when logarithmic axes are used. The number of wavelengths A_λ on the horizontal axes is defined as follows:

$$A_\lambda = \frac{l_{\mathrm{B}}}{\lambda_n} = \frac{l_{\mathrm{C}}}{\lambda_n}, \tag{29}$$

$$\lambda_n = \frac{2l_{\mathrm{ABC}}}{n}, \tag{30}$$

where λ_n is the wavelength of the highest *n*th-order eigenmode of the original acoustic field. As the number of wavelengths A_λ increased, the precision of the natural frequencies increased because of the variation in the phases of the eigenfunctions at $x = x_{\mathrm{B}}$ and x_{C}. However, when $A_\lambda > 2.2$ in Fig. 2(a) and $A_\lambda > 1.7$ in Fig. 2(b) were used, the precision of the natural frequencies decreased, and the lines were not smooth. This was because the condition number of the matrix in the eigenvalue analysis deteriorated. As the number of wavelengths A_λ increased, the condition number of the matrix deteriorated, and the precision of the natural frequencies decreased. The decrease in precision due to the matrix condition number depended on the software and functions used for the eigenvalue analysis. The eigs function of MATLAB was used for these simulations. In addition, the inverse of the mass matrix was multiplied by the left side of the stiffness matrix to perform an eigenvalue analysis as a standard eigenvalue problem. The results of the simulations in which the mass and stiffness matrices were separated and an eigenvalue analysis was performed as a generalized eigenvalue problem using MATLAB's eigs are presented in Fig. 3. Here, the simulation results of the RMS error rates of the natural frequencies corresponding to the simulation results presented in Figs. 2(a) and (b) are shown. Eigenvalue analysis, as a generalized eigenvalue problem, is less likely to cause matrix condition number problems and increases the precision of the natural frequencies. However, eigenvalue analysis, as a standard eigenvalue problem, is faster than eigenvalue analysis as a generalized eigenvalue problem. The computational time required for eigenvalue analysis is generally problematic. Therefore, it was performed as a standard eigenvalue problem in the subsequent simulations in this study. From the simulation results presented in Figs. 2 and 3, if A_λ is used for the evaluation, the tendency of the precision of the natural frequencies does not depend on *n*. From Fig. 2, the trend of the error rate of the first eigenmode is similar to that for multiple eigenmodes. Because both ends of the original acoustic field were closed, the natural frequencies were relatively precise, even near $A_\lambda = 0$, when the new boundaries were set to the closed ends. When the new boundaries were set to the closed ends, the precision was high for $A_\lambda = 0.5$. This was because the particle displacement of the highest *n*th-order eigenmode was zero for $x = x_{\mathrm{B}}$ and x_{C} when $A_\lambda = 0.5$ was used. This is advantageous for setting a new boundary with zero particle displacement at $x = x_{\mathrm{B}}$ and x_{C}. In Figs. 2(a) and (c), the error rate increases as *n* increases. This is because A_λ was used on the horizontal axes. If the elimination length $l_{\mathrm{B}} = l_{\mathrm{C}}$ is used rather than A_λ on the horizontal axes, the error rate decreases as *n* increases. In these simulations, the lengths of the elimination regions were varied while maintaining $l_{\mathrm{B}} = l_{\mathrm{C}}$. A similar tendency was observed when one length was

[DOI: 10.1299/mej.23-00241]

Table 1 Material properties used in the simulations for the verification on the length of the elimination region.

ρ_A	1.2 kg/m^3	$\rho_B = \rho_C$	0 kg/m^3
κ_A	138720 Pa	$\kappa_B = \kappa_C$	0 Pa
c_A	340 m/s	l_A	0.85 m

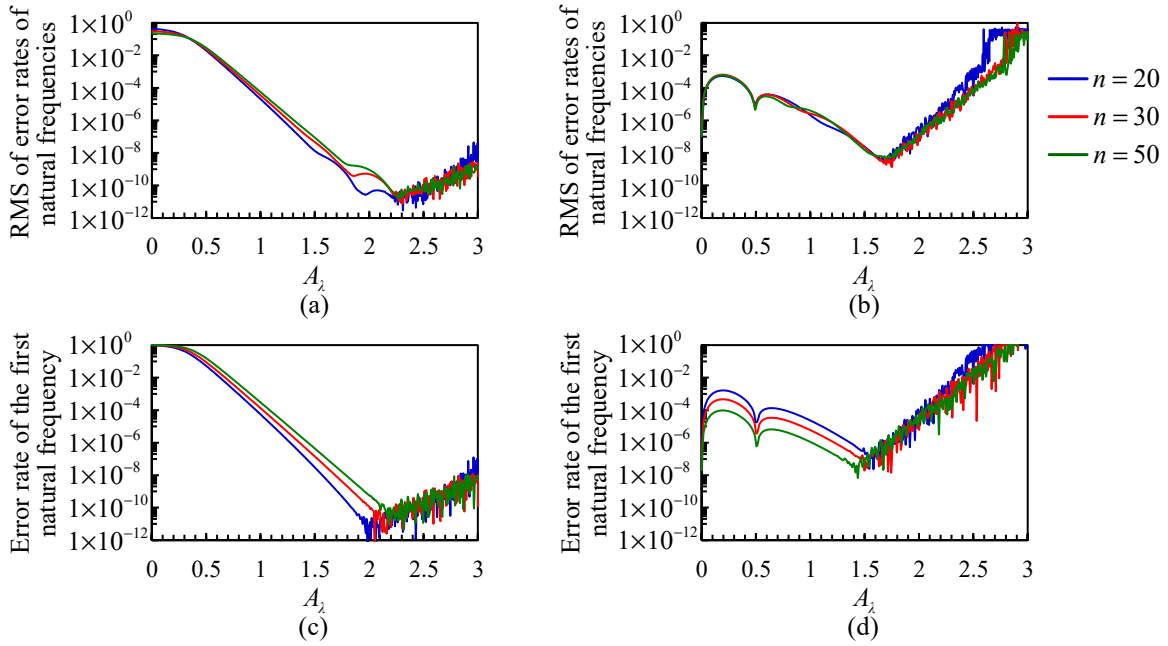

Fig. 2 Simulation results of the error rates of the natural frequencies obtained by the substructure elimination method using free or closed ends to the new boundaries. The eigenvalue analysis was performed as a standard eigenvalue problem. (a) RMS of the error rates of the multiple natural frequencies using free ends, (b) RMS of the error rates of the multiple natural frequencies using closed ends, (c) magnitude of the error rate of the first natural frequency using free ends, and (d) magnitude of the error rate of the first natural frequency using closed ends.

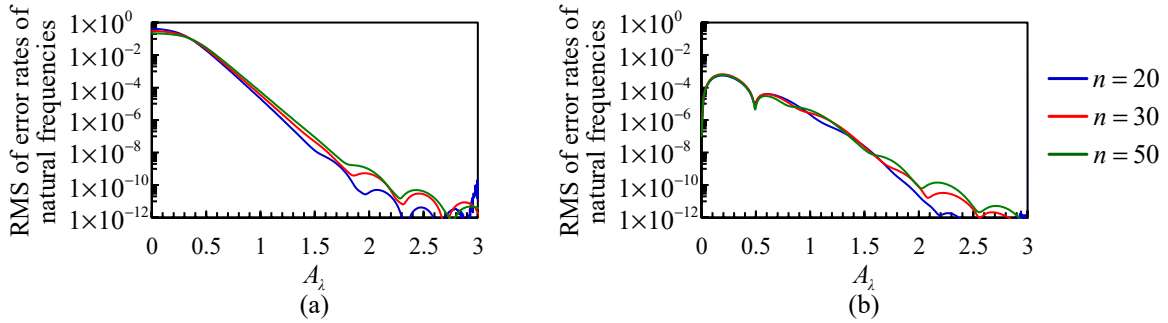

Fig. 3 Simulation results of the RMS of the error rates of the multiple natural frequencies obtained by the substructure elimination method using free or closed ends at the new boundaries. The eigenvalue analysis was performed as a generalized eigenvalue problem. (a) RMS of the error rates of the multiple natural frequencies using free ends and (b) RMS of the error rates of the multiple natural frequencies using closed ends.

fixed and the other was varied. However, the simulation results were omitted. In our simulation environment, A_λ should be selected such that $1.5 \le A_\lambda \le 2$. For example, when $A_\lambda = 2$ is used, the phase of the ith-order eigenmode is expressed as $4\pi i/n$ at $x = x_B$. Therefore, the phases of the zeroth- to nth-order eigenmodes at $x = x_B$ vary from 0 to 4π rad.

The 1st–8th-order eigenmodes for $n = 20$, 1st–16th-order eigenmodes for $n = 30$, and 1st–32nd-order eigenmodes for $n = 50$ were used in these simulations. Under the condition of $A_\lambda = 2.5$, the natural frequencies of the highest nth-order eigenmode of the original acoustic field were 2000, 4000, and 8000 Hz, respectively. Because these are equal to the natural frequencies of the 10th-, 20th-, and 40th-order eigenmodes of the acoustic field with the length $l_A = 0.85\,[\mathrm{m}]$,

[DOI: 10.1299/mej.23-00241]

the eigenmodes up to the 8th, 16th, and 32nd orders, which correspond to 80 % of them, were used. This is because these natural frequencies can be obtained with sufficient precision, which is discussed in Section 3.3.

3.2 Verification on density and bulk modulus of the elimination region

In the simulations whose results are presented in Section 3.1, both density and bulk modulus of the elimination regions were zero. In this section, the simulation results are presented for small values of density and bulk modulus of the elimination regions. The condition number of the matrix improved because of the small values. This occurred because the elimination regions also functioned as continuous bodies. However, the elimination regions also displayed mechanical impedance. This affected the precision of natural frequencies. The two boundary conditions described in Section 3.1 were used in these simulations. In principle, when the new boundary is a free end, the mechanical impedance of the elimination region affects the natural frequency. When it is a closed end, it does not affect the natural frequency.

The material properties of region A used in these simulations to verify the density and bulk modulus of the elimination region were identical to those listed in Table 1. The highest-order n of the eigenmode was 20 in these simulations. The simulation results for the magnitude of the error rate of the first-order natural frequency are presented in Fig. 4. The density ratio A_ρ and bulk modulus ratio A_κ are defined by the following equations:

$$A_\rho = \frac{\rho_\mathrm{B}}{\rho_\mathrm{A}} = \frac{\rho_\mathrm{C}}{\rho_\mathrm{A}}, \quad A_\kappa = \frac{\kappa_\mathrm{B}}{\kappa_\mathrm{A}} = \frac{\kappa_\mathrm{C}}{\kappa_\mathrm{A}}. \tag{31}$$

As can be observed in Eq. (31), $\rho_\mathrm{B} = \rho_\mathrm{C}$ and $\kappa_\mathrm{B} = \kappa_\mathrm{C}$ were used in these simulations. In addition, $A_\rho = A_\kappa$ was used. Under condition $A_\rho = A_\kappa$, the sound speeds of the center region and elimination regions are equal, and the precision of the natural frequencies is higher than that when the sound speeds are different. However, the small values of the density and bulk modulus in the elimination regions essentially reduced the precision of the natural frequencies even when the new boundaries were set to closed ends. When the new boundaries were set to closed ends, $A_\rho = A_\kappa = 1\times10^{-8}$ and 1×10^{-6} were more advantageous than $A_\rho = A_\kappa = 0$ with $A_\lambda > 1.8$. However, the elimination regions are relatively long under this condition. Consequently, the natural frequency of the highest nth-order eigenmode becomes relatively low. Therefore, a smaller A_λ is more advantageous to obtain a wide range of frequencies with a high precision. In Fig. 4(a), the precision is high at $A_\lambda = 2.5$. This is because the mechanical impedance of the elimination region is zero at 200 Hz. From Fig. 4(b), even when a closed end is set to the new boundary, eliminating substructures contributes to the improvement of precision. In principle, the mechanical impedance of the elimination region does not affect region A when the new boundaries are set to closed ends. However, because the elimination regions function as continuous bodies when the density and bulk modulus of the elimination regions have small values, the sound pressure should be expressed precisely in the elimination regions. This effect reduces the precision of natural frequencies of region A. Therefore, the elimination of substructures is effective for enhancing the precision in all the cases. Considering the results of this section and Section 3.1, it is the most effective to employ $A_\rho = A_\kappa = 0$ and $1.5 \le A_\lambda \le 2$, at least in the authors' simulation environment. When the problem of the condition number is more likely to occur compared with the authors' simulation environment, A_ρ and A_κ should have sufficiently small values to improve the condition number. In this case, the

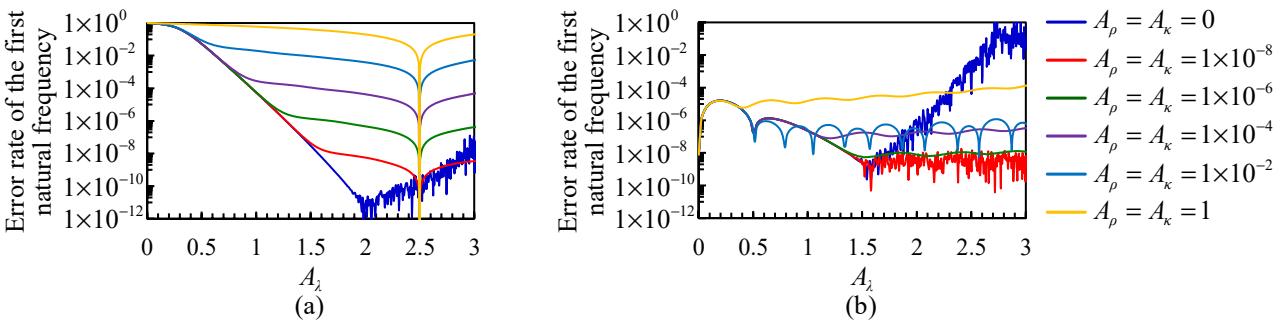

Fig. 4 Simulation results of the magnitude of the error rate of the first natural frequency obtained by the substructure elimination method using free or closed ends at the new boundaries. In these simulations, the densities and bulk moduli of the elimination regions are small. (a) Case where free ends are used and (b) case where closed ends are used.

[DOI: 10.1299/mej.23-00241]

results in Fig. 4 should be considered to determine the values of A_ρ and A_κ.

3.3 Verification to determine the highest order of the eigenmode of the original acoustic field

The frequency range in which the natural frequencies can be obtained with a high precision depends significantly on the natural frequency of the highest *n*th-order eigenmode of the original acoustic field. Simulations were conducted to investigate this frequency range. The boundary conditions in Section 3.1 were used in these simulations. The material properties used in the simulations are listed in Table 2. These material properties were also used in the simulations whose results are presented in Section 3.4. The cross-sectional area S affects only the results of the simulations performed for the verification in Section 3.4. The natural frequencies of the original acoustic fields are integer multiples of $1200/14 \approx 85.7$ (Hz). Therefore, the natural frequency of the highest 14th-order eigenmode of the original acoustic field was 1200 Hz in these simulations. The natural frequencies obtained using MATLAB's eigenvalue analysis are listed in Table 3. In both the cases, the natural frequency of 0 Hz owing to the zeroth-order eigenmode of the original acoustic field was omitted from Table 3. As the zeroth-order eigenmode of the original acoustic field is essentially uncoupled, a natural frequency of 0 Hz always appears. The natural frequencies were listed as the lowest digits obtained using MATLAB, except when the exact natural frequency was 0 Hz. The error rates were listed in three digits. When the new boundaries were set to the closed ends, the precision of the two natural frequencies of 600 Hz and 1200 Hz was significantly higher than that of the others. This was because the original acoustic field had eigenmodes with natural frequencies of 600 and 1200 Hz, and the particle displacements of these eigenmodes were zero at the new boundaries. When the new boundaries were set at the closed ends, the simulation results exhibited two extraordinarily high natural frequencies. A number of natural frequencies equal to that of the closed ends was obtained using the substructure elimination method. In both the cases, the precision of the natural frequencies varied significantly at approximately 1200 Hz. Therefore, the frequency range in which the natural frequencies can be obtained with a high precision is less than that of the highest *n*th-order eigenmode of the original acoustic field. When the frequency range should be limited

Table 2 Material properties used in the simulations for the verification to determine the highest-order of the eigenmode of the original acoustic field.

ρ_A	1.2 kg/m^3	$\rho_B = \rho_C$	0 kg/m^3
κ_A	138720 Pa	$\kappa_B = \kappa_C$	0 Pa
c_A	340 m/s	$l_B = l_C$	$2l_A/3$ m
l_A	0.85 m	A_λ	2
S	15000 mm^2	n	14

Table 3 Natural frequencies obtained by MATLAB's eigenvalue analysis and their error rates. The natural frequency of the highest *n*th-order eigenmode of the original acoustic field was 1200 Hz in these simulations.

Case where new boundaries were set to free ends			Case where new boundaries were set to closed ends		
Exact natural frequencies [Hz]	Calculated natural frequencies [Hz]	Error rate [%]	Exact natural frequencies [Hz]	Calculated natural frequencies [Hz]	Error rate [%]
0	0.00034669899379	-	200	199.999535045785	-2.32×10^{-4}
200	200.000000000929	4.64×10^{-10}	400	400.001690579893	4.23×10^{-4}
400	399.999999999779	-5.52×10^{-11}	600	600.000000000016	2.71×10^{-12}
600	600.000000002402	4.00×10^{-10}	800	800.001589371674	1.99×10^{-4}
800	800.000000010366	1.30×10^{-9}	1000	1000.00022548121	2.25×10^{-5}
1000	1000.00000001825	1.83×10^{-9}	1200	1200.00000000000	3.33×10^{-13}
1200	1200.00061545947	5.13×10^{-5}	1400	1400.28529686949	2.04×10^{-2}
1400	1400.01473512633	1.05×10^{-3}	1600	1599.8235058131	-1.10×10^{-2}
1600	1607.63239823502	4.77×10^{-1}	1800	1864.4321280439	3.58
1800	1817.31035967686	9.62×10^{-1}	2000	2111.99681018905	5.60
2000	2294.41154083378	14.7	2200	3224.32583664127	46.6
2200	2610.78412243085	18.7	2400	3691.64295211865	53.8
2400	6186.09007335966	158	2600	1259397.78781721	4.83×10^{4}
2600	7134.20738912921	174	2800	2288087.86470475	8.16×10^{4}

[DOI: 10.1299/mej.23-00241]

to a higher precision, the upper limit of the frequency range should be 0.9 or 0.8 times the highest *n*th-order natural frequency, rather than one time the highest *n*th-order natural frequency.

In the simulation using the substructure elimination method, the elimination length $l_B = l_C$ and highest-order n of the eigenmode of the original acoustic field should be determined. Because the natural frequency of the highest *n*th-order eigenmode depends on both $l_B = l_C$ and n, the natural frequency of the highest *n*th-order eigenmode is tentatively defined as $f_{n\mathrm{T}}$. The natural frequency $f_{n\mathrm{T}}$ and elimination length $l_B = l_C$ are expressed as

$$f_{n\mathrm{T}} = \frac{nc_A}{2l_{ABC}}, \tag{32}$$

$$l_B = l_C = A_{\lambda\mathrm{T}}\lambda_n, \tag{33}$$

where $A_{\lambda\mathrm{T}}$ is the tentative number of wavelengths. Because l_A and c_A are given and $A_{\lambda\mathrm{T}}$ and $f_{n\mathrm{T}}$ are arbitrarily determined by the user, from Eqs. (30), (32), and (33), the elimination length $l_B = l_C$ can be derived as

$$l_B = l_C = A_{\lambda\mathrm{T}}\frac{c_A}{f_{n\mathrm{T}}}. \tag{34}$$

From Eqs. (32) and (34), the highest-order n of the eigenmode of the original acoustic field can be derived as

$$n = \left\lceil \frac{2f_{n\mathrm{T}}l_A}{c_A} + 4A_{\lambda\mathrm{T}} \right\rceil, \tag{35}$$

where the ceiling function was used to make n an integer. Because the elimination length $l_B = l_C$ and highest-order n are determined by Eqs. (34) and (35), respectively, the true natural frequency of the highest *n*th-order eigenmode and true number of wavelengths are given by the following equations:

$$f_n = f_{n\mathrm{T}}\frac{\left\lceil \frac{2f_{n\mathrm{T}}l_A}{c_A} + 4A_{\lambda\mathrm{T}} \right\rceil}{\frac{2f_{n\mathrm{T}}l_A}{c_A} + 4A_{\lambda\mathrm{T}}}, \quad A_\lambda = A_{\lambda\mathrm{T}}\frac{\left\lceil \frac{2f_{n\mathrm{T}}l_A}{c_A} + 4A_{\lambda\mathrm{T}} \right\rceil}{\frac{2f_{n\mathrm{T}}l_A}{c_A} + 4A_{\lambda\mathrm{T}}}. \tag{36}$$

Because of the rounding off of n in Eq. (35), f_n and A_λ are marginally higher than $f_{n\mathrm{T}}$ and $A_{\lambda\mathrm{T}}$, respectively. When $f_{n\mathrm{T}}$ and $A_{\lambda\mathrm{T}}$ are selected such that the ceiling function part in Eq. (35) is an integer, this difference does not occur.

3.4 Verification of the relationship between the degrees of freedom and precision

The relationship between the degrees of freedom and precision was investigated by comparing the simulation results of modal analysis with and without the substructure elimination method. To verify the effectiveness of the formulations for installing the displacement excitation and 1-DOF vibration systems at the new boundaries, the analytical model in which the displacement excitation and 1-DOF vibration systems were set to the new boundaries was used in these simulations. The simulation results of modal analysis with and without the substructure elimination method are evaluated based on the exact solution derived using the boundary conditions.

3.4.1 Analytical model used in the simulation

The analytical model used in the simulations are shown in Fig. 5. Here, the boundary conditions on the left and right ends are the displacement excitation and 1-DOF vibration system, respectively. The symbols used in the acoustic field are common to region A in the analytical model shown in Fig. 1. The left end of the acoustic field is set to the origin of the x'-coordinate, and the right-hand direction is the positive direction of the x'-coordinate. In the analytical model shown in Fig. 1, the displacement excitation of the piston is installed at $x = x_B$. Therefore, the relationship between x and x' is expressed as $x = x' + x_B$. The material properties of the acoustic field used in these simulations are identical to those listed in Table 2. In the simulation using the substructure elimination method, the natural frequency of the highest

[DOI: 10.1299/mej.23-00241]

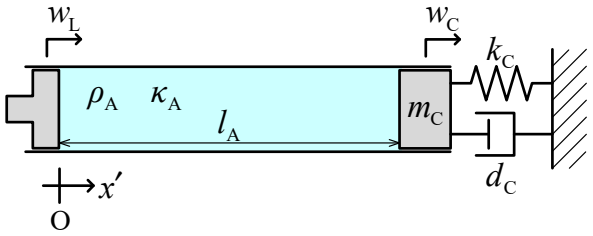

Fig. 5 Analytical model where a piston for the displacement excitation and 1-DOF vibration system are installed at the left and right ends, respectively.

*n*th-order eigenmode was 1200 Hz. In the simulation using conventional modal analysis without the substructure elimination method, the highest order of the eigenmode was set to the 14th. Therefore, the natural frequency of the highest *n*th-order eigenmode was 2800 Hz using the conventional method. The material properties of the 1-DOF vibration system are listed in Table 4. Here, j is the imaginary unit, and β_z is the characteristic impedance ratio, and is defined as

$$\beta_z = \begin{cases} \dfrac{1}{S}\sqrt{\dfrac{m_C k_C}{\rho_A \kappa_A}} & \text{(Case (1) and (2))} \\ \dfrac{d_C}{S\sqrt{\rho_A \kappa_A}} & \text{(Case (3))} \end{cases}, \tag{37}$$

where $\sqrt{\rho_A \kappa_A}\,(=\rho_A c_A)$ is the characteristic impedance of air. As listed in Table 4, three material properties were used in the 1-DOF vibration system. In Cases (1) and (2), the damping coefficients of the dashpot were zero. Therefore, the eigenvalue analysis could be applied to the equations of motion. In Case (3), only the damping coefficient was applied to make the right end a non-reflective boundary. Specifically, it is not a vibration system because it does not have a natural frequency. In this case, the equations of state were derived, an eigenvalue analysis was performed, and the equations were decoupled.

Table 4 Material properties of the 1-DOF vibration systems used in the simulations for verifying the relationship between the degrees of freedom and precision.

	Case (1)	Case (2)	Case (3)
m_C [g]	50	0.5	0
d_C [Ns/m]	0	0	$6.12\left(=\sqrt{\rho_A \kappa_A}S\right)$
k_C [N/m]	$3\times10^5\,(1+0.1\mathrm{j})$	$3\times10^3\,(1+0.1\mathrm{j})$	0
β_z	$20(1+0.050\mathrm{j})$	$0.20(1+0.050\mathrm{j})$	1

3.4.2 Derivation of the exact solution using boundary conditions

The wave equation for the analytical model shown in Fig. 5 is expressed as follows:

$$\rho_A \frac{\partial^2 \psi}{\partial t^2} = \kappa_A \frac{\partial^2 \psi}{\partial x'^2}. \tag{38}$$

From wave equation (38), the displacement potential $\psi(x', t)$ is derived as

$$\psi(x', t) = \Psi(x')\mathrm{e}^{\mathrm{j}\omega t},\quad \Psi(x') = C_1 \cos kx' + C_2 \sin kx',\quad k = \frac{\omega}{c_A}, \tag{39}$$

where ω is the excitation angular frequency, k is the wave number, and C_1 and C_2 are constants determined by the boundary conditions. The boundary condition at the left end is the displacement $w_L = W_L \mathrm{e}^{\mathrm{j}\omega t}$. Here, W_L is the amplitude of w_L. The boundary condition at the right end is the mechanical impedance. It is given by the following equation:

[DOI: 10.1299/mej.23-00241]

$$z_{\mathrm{C}} = \mathrm{j}\omega m_{\mathrm{C}} + d_{\mathrm{C}} + \frac{k_{\mathrm{C}}}{\mathrm{j}\omega}. \tag{40}$$

Using Eq. (39) and two boundary conditions, C_1 and C_2 are obtained as follows:

$$C_1 = \frac{W_{\mathrm{L}}}{k}\frac{\mathrm{j}\rho_{\mathrm{A}}c_{\mathrm{A}}\sin kl_{\mathrm{A}} + \dfrac{z_{\mathrm{C}}}{S}\cos kl_{\mathrm{A}}}{\mathrm{j}\rho_{\mathrm{A}}c_{\mathrm{A}}\cos kl_{\mathrm{A}} - \dfrac{z_{\mathrm{C}}}{S}\sin kl_{\mathrm{A}}}, \quad C_2 = -\frac{W_{\mathrm{L}}}{k}. \tag{41}$$

The sound pressure and particle displacement are expressed as

$$p(x',t) = \rho_{\mathrm{A}}\frac{\partial^2\psi}{\partial t^2} = -\omega^2\rho_{\mathrm{A}}\left(C_1\cos kx' + C_2\sin kx'\right)\mathrm{e}^{\mathrm{j}\omega t}, \quad w(x',t) = -\frac{\partial\psi}{\partial x'} = k\left(C_1\sin kx' - C_2\cos kx'\right)\mathrm{e}^{\mathrm{j}\omega t}, \tag{42}$$

respectively. Equation (42) is the exact solutions for the sound pressure and particle displacement, respectively. Exact solutions can be obtained using this method. However, equations of motion with low DOFs cannot be obtained because this method does not derive an equation of motion for each eigenmode.

3.4.3 Conventional modal analysis without using the substructure elimination method

Replacing the displacement excitation at both ends of the acoustic field with rigid walls and sound pressure sources (Yamada and Utsuno, 2015, 2020), the wave equation is obtained as follows:

$$\rho_{\mathrm{A}}\frac{\partial^2\psi}{\partial t^2} = \kappa_{\mathrm{A}}\frac{\partial^2\psi}{\partial x'^2} + \kappa_{\mathrm{A}}w_{\mathrm{L}}\delta(x') - \kappa_{\mathrm{A}}w_{\mathrm{C}}\delta(x' - l_{\mathrm{A}}). \tag{43}$$

In the conventional modal analysis without using the substructure elimination method, the displacement potential is given as

$$\psi(x',t) = \sum_{h=0}^{n}\Psi'_h(x')\xi'_h(t), \quad \Psi'_h(x') = A'_h\cos k'_h x', \quad k'_h = \frac{h\pi}{l_{\mathrm{A}}}, \tag{44}$$

where Ψ'_h is the eigenfunction of the displacement potential, ξ'_h is the modal displacement, A'_h is an arbitrary constant, and k'_h is the wave number. The sound pressure and particle displacement are expressed as

$$p(x',t) = \rho_{\mathrm{A}}\frac{\partial^2\psi}{\partial t^2}, \tag{45}$$

$$w(x',t) = -\frac{\partial\psi}{\partial x'}, \tag{46}$$

respectively. The Gibbs phenomenon occurs during particle displacement, as derived using Eqs. (44) and (46). To solve this problem, the particle displacement derived by integrating both sides of the wave equation (43) from $x' = 0$ to x' should be used. The particle displacement is expressed as

$$w(x',t) = -\frac{\partial\psi}{\partial x'} = w_{\mathrm{L}}H(x') - \frac{1}{c_{\mathrm{A}}^2}\int_0^{x'}\frac{\partial^2\psi}{\partial t^2}\mathrm{d}x'. \tag{47}$$

Substituting Eq. (44) into wave equation (43), multiplying both sides by $\Psi'_i/\rho_{\mathrm{A}}$, and integrating over the entire range of the acoustic field, we obtain the following equations of motion using modal displacements:

[DOI: 10.1299/mej.23-00241]

$$M_i'\ddot{\xi}_i' + K_i'\xi_i' + c_{\mathrm{A}}^2\Psi_i'(l_{\mathrm{A}})w_{\mathrm{C}} = c_{\mathrm{A}}^2\Psi_i'(0)w_{\mathrm{L}}\,, \tag{48}$$

$$M_i' = \int_0^{l_{\mathrm{A}}}\Psi_i'^2\mathrm{d}x' = 1\,,\quad K_i' = -c_{\mathrm{A}}^2\int_0^{l_{\mathrm{A}}}\Psi_i'\frac{\mathrm{d}^2\Psi_i'}{\mathrm{d}x'^2}\mathrm{d}x' = \omega_i'^2\,,\quad \omega_i' = \frac{i\pi c_{\mathrm{A}}}{l_{\mathrm{A}}}\,,\quad A_i' = \begin{cases}\sqrt{\dfrac{1}{l_{\mathrm{A}}}} & (i=0)\\ \sqrt{\dfrac{2}{l_{\mathrm{A}}}} & (i=1,\,2,\,\cdots)\end{cases}\,, \tag{49}$$

where M_i' and K_i' are the modal mass and stiffness, respectively, and ω_i' is the natural angular frequency of the *i*th-order eigenmode. The arbitrary constant A_i' of the eigenfunction was normalized such that $M_i' = 1$. The equation of motion of the 1-DOF vibration system is derived as

$$m_{\mathrm{C}}\ddot{w}_{\mathrm{C}} + d_{\mathrm{C}}\dot{w}_{\mathrm{C}} + k_{\mathrm{C}}w_{\mathrm{C}} = Sp(l_{\mathrm{A}}, t)\,, \tag{50}$$

where the force term on the right-hand side can be expressed by the superposition of the eigenmodes using Eqs. (44) and (45). The equations of motion using matrices can be obtained using Eqs. (48) and (50). This conventional method is categorized as a substructure synthesis method. The subsequent modal analysis is identical to that performed using the substructure elimination method. In the simulation using the material properties of Case (3), where only the damping coefficient is given, from Eqs. (45) and (50), the displacement w_{C} is obtained as

$$w_{\mathrm{C}} = \frac{S\rho_{\mathrm{A}}}{d_{\mathrm{C}}}\frac{\partial\psi}{\partial t}\bigg|_{x'=l_{\mathrm{A}}}\,. \tag{51}$$

When the damping coefficient is given, the eigenvalue analysis should be performed after the equation of state for state-space representation is obtained.

3.4.4 Simulation results

The simulation results of the nondimensional sound pressure and particle displacement at $x = x_{\mathrm{B}}$ and $x = x_{\mathrm{B}} + 0.7l_{\mathrm{A}}$ are presented in Fig. 6. Here, P is the complex amplitude of the sound pressure p, and W is the complex amplitude of the particle displacement w. The material properties of Case (1) listed in Table 4 were used for the 1-DOF vibration system. Moreover, dashed lines were drawn at 1200 Hz of the natural frequency of the highest *n*th-order eigenmode in the substructure elimination method. The 400 Hz resonance peak was suppressed by the 1-DOF vibration system. The simulation results of modal analysis with and without the substructure elimination method agreed well with the exact solutions near the resonance peaks. The precision of the simulation results obtained using the proposed method was insufficient above 1200 Hz. Conversely, the precision of the conventional method without the substructure elimination method was high even above 1200 Hz. This was because the natural frequency of the highest *n*th-order eigenmode was 2800 Hz in the conventional method. However, the simulation results of the nondimensional sound pressure obtained using the conventional method do not agree well with the exact solution near the anti-resonance points when the evaluation point is $x = x_{\mathrm{B}}$. Because the eigenfunctions used in the conventional method do not exhibit phase variation at $x = x_{\mathrm{B}}$, the precision decreases near $x = x_{\mathrm{B}}$. This problem did not occur when the substructure elimination method was used. The simulation result of the particle displacement did not exhibit this problem even for the conventional method because Eq. (47) was used.

The simulation results for the nondimensional sound pressure and particle displacement using the material properties of Case (2) are presented in Fig. 7. The characteristic impedance ratio β_z in Case (2) was smaller than that in Case (1). The simulation results of the conventional method did not agree with the exact solution. Even the natural frequencies obtained using the conventional method did not agree with the exact solution. Because the conventional method uses eigenfunctions when both ends are closed, the precision of the simulations was high when the mechanical impedance of the 1-DOF vibration system was large. However, the error increased when the mechanical impedance of the 1-DOF vibration system was small. β_z can be used as a criterion for determining the magnitude of the mechanical impedance. The number of eigenmodes should be increased to increase the precision of the conventional methods. Conversely, the simulation results of the proposed method agreed well with the exact solutions below 1200 Hz. This was because the

[DOI: 10.1299/mej.23-00241]

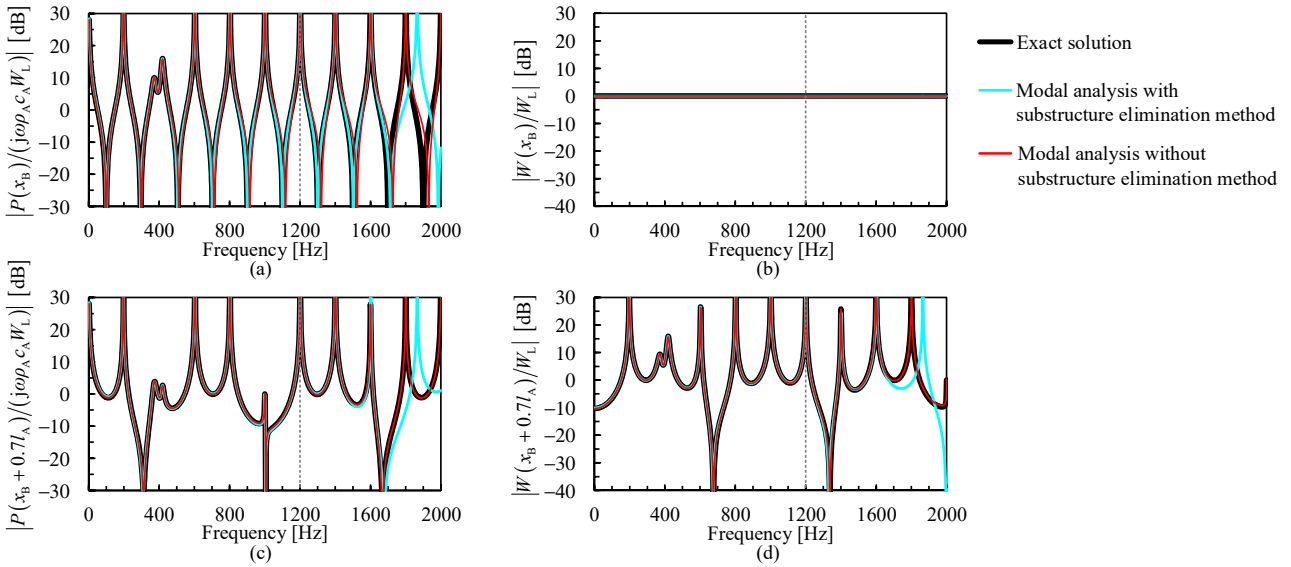

Fig. 6 Simulation results of nondimensional sound pressure and particle displacement at $x = x_B$ and $x_B + 0.7l_A$ when the material properties of Case (1), listed in Table 4, were used: (a) nondimensional sound pressure at $x = x_B$, (b) nondimensional particle displacement at $x = x_B$, (c) nondimensional sound pressure at $x = x_B + l_A$ and (d) nondimensional particle displacement at $x = x_B + l_A$.

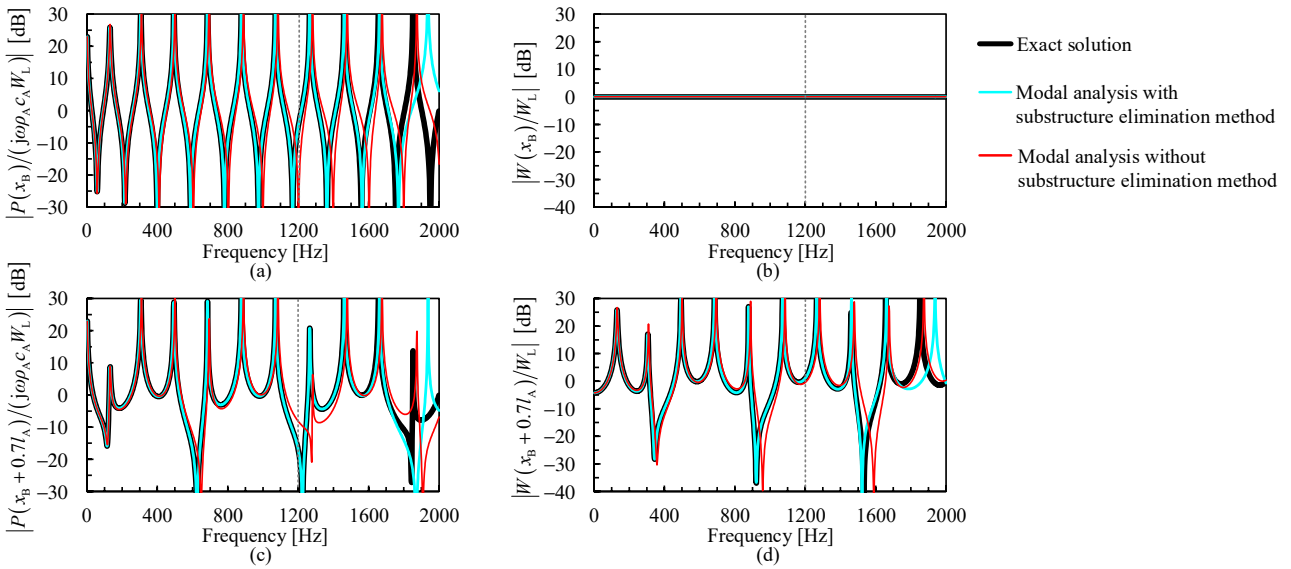

Fig. 7 Simulation results of nondimensional sound pressure and particle displacement at $x = x_B$ and $x_B + 0.7l_A$ when the material properties of Case (2), listed in Table 4, were used: (a) nondimensional sound pressure at $x = x_B$, (b) nondimensional particle displacement at $x = x_B$, (c) nondimensional sound pressure at $x = x_B + l_A$ and (d) nondimensional particle displacement at $x = x_B + l_A$.

eigenfunctions used in the proposed method displayed a large phase variation at $x = x_C$. In the proposed method, the phases of the zeroth- to 14th-order eigenmodes at $x = x_C$ vary from 0 to 10π rad at regular intervals. In the conventional method, they repeat alternately in-phase and anti-phase. Therefore, the proposed method has 14 types of phases, and the conventional method has 2 types of phases.

The simulation results for the nondimensional sound pressure and particle displacement using the material properties of Case (3) are presented in Fig. 8. Because the right end is a non-reflective boundary in Case (3), $\beta_z = 1$. Owing to the small phase variation, the simulation results obtained using the conventional method did not agree with the exact solutions. The simulation results using the conventional method with the 0th–140th eigenmodes are presented in Fig. 8. Even when the number of eigenmodes was increased by an order of magnitude, the precision of the conventional method was lower than that of the proposed method. The simulation results of the proposed method agreed well with the exact

[DOI: 10.1299/mej.23-00241]

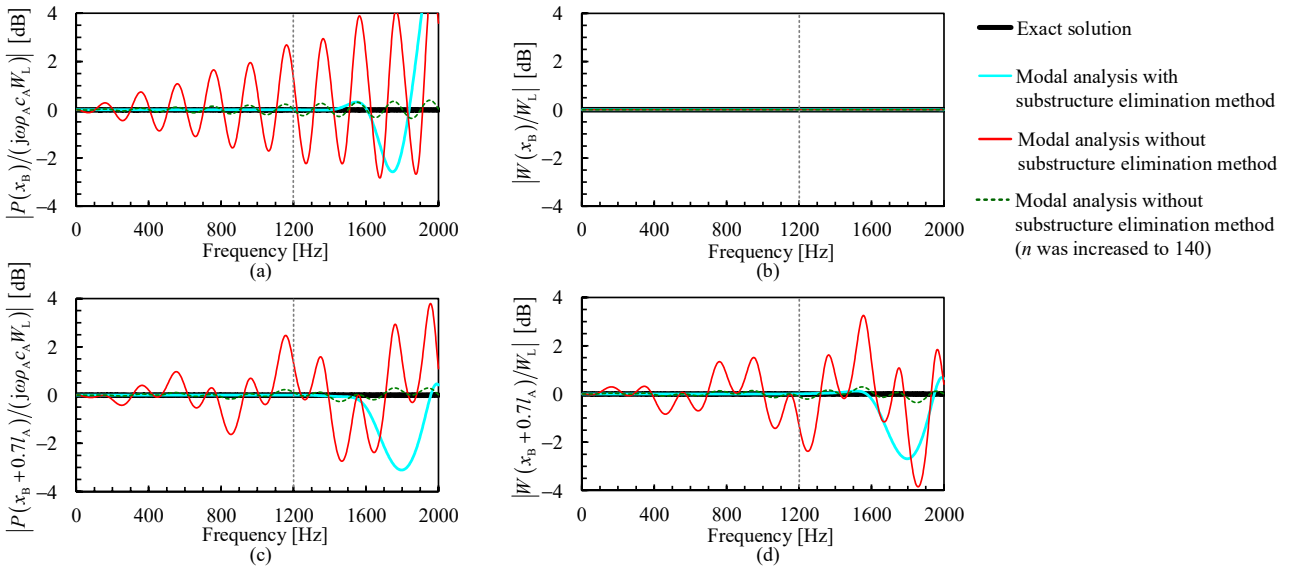

Fig. 8 Simulation results of nondimensional sound pressure and particle displacement at $x = x_B$ and $x_B + 0.7l_A$ when the material properties of Case (3), listed in Table 4, were used: (a) nondimensional sound pressure at $x = x_B$, (b) nondimensional particle displacement at $x = x_B$, (c) nondimensional sound pressure at $x = x_B + l_A$ and (d) nondimensional particle displacement at $x = x_B + l_A$.

solutions below 1200 Hz. The large phase variation at $x = x_C$ was effective under this condition.

4. Conclusion

The substructure elimination method for a continuous body governed by a one-dimensional wave equation was described using a one-dimensional acoustic field as a representative. New formulations, based on constraint conditions, were proposed as versatile methods for setting arbitrary boundary conditions for new boundaries. The formulations for installing a free end, closed end, displacement excitation and arbitrary mechanical impedance using a 1-DOF vibration system on a new boundary were described. The simulations revealed that the density and bulk modulus of the elimination region should be zero if the deterioration of the matrix condition number is not problematic. These also revealed that the length of the elimination region should be set at 1.5–2 times the wavelength of the highest eigenmode when the eigenvalue analysis is performed as a standard eigenvalue problem using an inverse matrix of the mass matrix in the simulations using MATLAB. The precision of the simulations can be enhanced by further lengthening the elimination region of a simulation environment in which the condition number of the matrices is less problematic than that of the authors. In this study, formulations to determine the length of the elimination region and the order of the highest-order eigenmode were derived based on the upper limit of the frequency range. The precision of the sound pressure near the displacement excitation boundary was enhanced when the substructure elimination method was used, compared with conventional modal analysis using the substructure synthesis method. Modal analysis using the substructure elimination method is more advantageous than that of the conventional method. The exception is when the installed mechanical impedance is considered sufficiently large with respect to the characteristic impedance of air.

Acknowledgment

This work was partially supported by a Grant-in-Aid for Scientific Research (C) (JSPS KAKENHI Grant Number JP21K03956) and financially supported partially by the Kansai University Fund for Domestic and Overseas Research Fund, 2022. This research was conducted while the first author stayed at the University of Technology Sydney as a visiting professor. The authors are grateful to the university for this appointment.

References

Benaroya, H. and Nagurka, M. L., Mechanical Vibration: Analysis, Uncertainties, and Control, Third edition (2009),

CRC Press.
Bishop, R. E. D. and Johnson, D. C., The Mechanics of Vibration (1960), Cambridge University Press.
Hale, A. L. and Meirovitch, L., A general substructure synthesis method for the dynamic simulation of complex structures, Journal of Sound and Vibration, Vol. 69, Issue 2(1980), pp. 309–326.
Jiménez, N., Umnova, O., and Groby, JP, Acoustic Waves in Periodic Structures, Metamaterials, and Porous Media (2021), Springer, Cham.
Meirovitch, L., Analytical Methods in Vibrations (1967), Macmillan.
Meirovitch, L., Dynamics and Control of Structures (1990), John Wiley & Sons.
Meirovitch, L., Fundamentals of Vibrations (2001), McGraw-Hill Higher Education.
Nagamatsu, A., Modal Analysis (1985), Baifukan (in Japanese).
Ohtomi, K., Kansei modeling for delight design based on 1DCAE concept, Proceedings of the 11th International Modelica Conference (2015), pp. 811–815.
Ookuma, M. and Nagamatsu, A., Vibration analysis by substructure synthesis method (Part 4, Calculation of residual compliance matrix), Bulletin of the Japan Society of Mechanical Engineers, Vol. 28, No. 239(1985), pp. 905–910.
Ookuma, M. and Nagamatsu, A., Vibration analysis by component mode synthesis method (Comparison of three methods (I)), Bulletin of the Japan Society of Mechanical Engineers, Vol. 29, No. 249(1986), pp. 882–887.
Rao, S. S., Vibration of Continuous Systems (2007), John Wiley & Sons.
Reismann, H., Elastic Plates: Theory and Application (1988), John Wiley & Sons.
Shabana, A. A., Substructure synthesis methods for dynamic analysis of multi-body systems, Computers & Structures, Vol. 20, No. 4(1985), pp. 737–744.
Shabana, A. A., Theory of Vibration: Volume II: Discrete and Continuous Systems (1991), Springer-Verlag New York, Inc.
Shigeno, Y. and Yamada, K., Broadening of frequency range of wave cancellation by unidirectional traveling wave using feedback comb filter, SICE System Integration Division Annual Conference (2022), pp. 760–765 (in Japanese).
Tanaka, N., Takara, Y., and Iwamoto, H., Eigenpairs of a coupled rectangular cavity and its fundamental properties, Journal of the Acoustical Society of America, Vol. 131, No. 3(2012), pp. 1910–1921.
Uhrig, R., The transfer matrix method seen as one method of structural analysis among others, Journal of Sound and Vibration, Vol. 4, Issue 2(1966), pp. 136–148.
Yamada, K., Proposal of substructure change or elimination method, Dynamics and Design Conference (2017), p. 440(12 pages) (in Japanese).
Yamada, K., Vibration analysis using substructure change and elimination methods, Proceedings of the 25th International Congress on Sound and Vibration (2018), p. 485(8 pages).
Yamada, K., Shimizu, T., Utsuno, H., Kurata, J., and Murakami, Y., Optimum tuning of damped side-branch silencer using equivalent discrete model and considering open-end correction, Mechanical Engineering Journal, Vol. 8, No. 1(2021), DOI: 10.1299/mej.20-00417.
Yamada, K., Shimizu, T., Utsuno, H., Kurata, J., and Murakami, Y., Optimum tuning of damped Helmholtz silencer using an equivalent discrete model and considering open-end correction, Mechanical Engineering Journal, Vol. 8, No. 4(2021), DOI: 10.1299/mej.21-00139.
Yamada, K. and Utsuno, H., Theoretical analysis of vibration of continuous body using replacement of displacement excitation with force excitation, Proceedings of the 22nd International Congress on Sound and Vibration (2015), p. 428(8 pages).
Yamada, K. and Utsuno, H., Modal analysis of continuous systems by replacing displacement excitation with equivalent excitation force and fixed boundary, Mechanical Engineering Journal, Vol. 7, No. 4(2020), DOI: 10.1299/mej.20-00003.

[DOI: 10.1299/mej.23-00241]